nature nanotechnology

SUPPLEMENTARY INFORMATION

https://doi.org/10.1038/s41565-018-0319-4

In the format provided by the authors and unedited.

In situ sprayed bioresponsive immunotherapeutic gel for post-surgical cancer treatment

Qian Chen[1,2,3], Chao Wang[3], Xudong Zhang[1,2], Guojun Chen[1,2], Quanyin Hu[1,2,3], Hongjun Li[4], Jinqiang Wang[3], Di Wen[1,2], Yuqi Zhang[3], Yifei Lu[3,5], Guang Yang[1,2], Chen Jiang[5], Jun Wang[4], Gianpietro Dotti[6] and Zhen Gu[1,2,3,7,8]*

[1]Department of Bioengineering, University of California, Los Angeles, CA, USA. [2]California NanoSystems Institute, University of California, Los Angeles, CA, USA. [3]Joint Department of Biomedical Engineering, University of North Carolina at Chapel Hill and North Carolina State University, Raleigh, NC, USA. [4]National Engineering Research Center for Tissue Restoration and Reconstruction, and School of Biomedical Science and Engineering, South China University of Technology, Guangzhou, Guangdong, China. [5]Key Laboratory of Smart Drug Delivery, Ministry of Education, State Key Laboratory of Medical Neurobiology, Department of Pharmaceutics, School of Pharmacy, Fudan University, Shanghai, China. [6]Lineberger Comprehensive Cancer Center, University of North Carolina, Chapel Hill, NC, USA. [7]Jonsson Comprehensive Cancer Center, University of California, Los Angeles, CA, USA. [8]Center for Minimally Invasive Therapeutics, University of California, Los Angeles, CA, USA. *e-mail: guzhen@ucla.edu

Supporting Information

In Situ Sprayed Bioresponsive Immunotherapeutic Gel for Post-Surgical Cancer Treatment

Qian Chen[1, 2, 3], Chao Wang[3], Xudong Zhang[1, 2], Guojun Chen[1, 2], Quanyin Hu[1, 2, 3], Hongjun Li[4], Jinqiang Wang[3], Di Wen[1, 2], Yuqi Zhang[3], Yifei Lu[3, 5], Guang Yang[1, 2], Chen Jiang[5], Jun Wang[4], Gianpietro Dotti[6], and Zhen Gu[1, 2, 3, 7, 8]∗

1 Department of Bioengineering, University of California, Los Angeles, California 90095, United States

2 California NanoSystems Institute, University of California, Los Angeles, California 90095, United States

3 Joint Department of Biomedical Engineering, University of North Carolina at Chapel Hill and North Carolina State University, Raleigh, North Carolina 27695, United States

4 National Engineering Research Center for Tissue Restoration and Reconstruction, and School of Biomedical Science and Engineering, South China University of Technology, Guangzhou, Guangdong 510006, China

5 Key Laboratory of Smart Drug Delivery, Ministry of Education, State Key Laboratory of Medical Neurobiology, Department of Pharmaceutics, School of Pharmacy, Fudan University, Shanghai 201203, China

6 Lineberger Comprehensive Cancer Center, University of North Carolina, Chapel Hill, North Carolina 27599, United States

7 Jonsson Comprehensive Cancer Center, University of California, Los Angeles, California 90095, United States

8 Center for Minimally Invasive Therapeutics, University of California, Los Angeles, California 90095, United States

* Corresponding author: E-mail: guzhen@ucla.edu

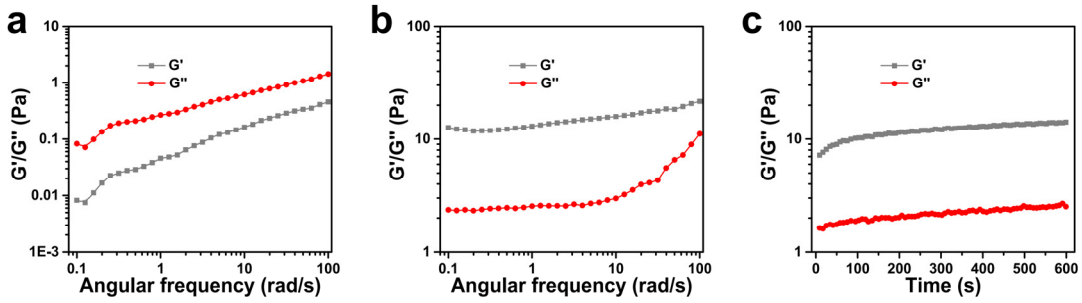

Supplementary Fig. 1. Dynamic rheological behavior of fibrinogen before and after gelation at 25 °C measured using a TA Instruments AR-2000 stress controlled rheometer with the 25 mm aluminum cross-hatched parallel plates. All experiments were conducted in the linear viscoelastic regime with a 500 μm gap between the plates and conducted at least triplicate measurements. (a) Frequency spectra of the elastic (G′) and viscous (G″) moduli of fibrinogen containing IgG@$CaCO_3$ NPs samples with the exhibiting solution-like characteristics. (b) Frequency spectra of the elastic (G′) and viscous (G″) moduli of IgG@$CaCO_3$@fibrin samples showing a gel-like behavior. (c) Evaluation of G′ and G″ as a function of time of mixing of fibrinogen containing IgG@$CaCO_3$ (IgG: Immunoglobulin G) and thrombin showing ultrafast sol-gel transition. The experiments were repeated three times.

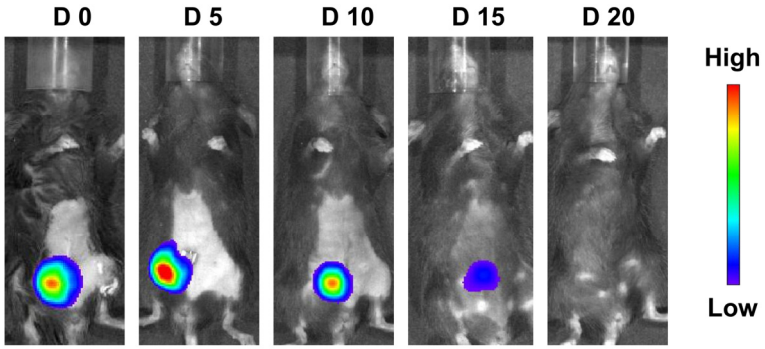

Supplementary Fig. 2. *In vivo* gel degradation. The fibrinogen conjugated with Cy5.5 and thrombin was sprayed within the resected tumor site. The fluorescence IVIS imaging was performed at the indicated time points. The experiments were repeated three times.

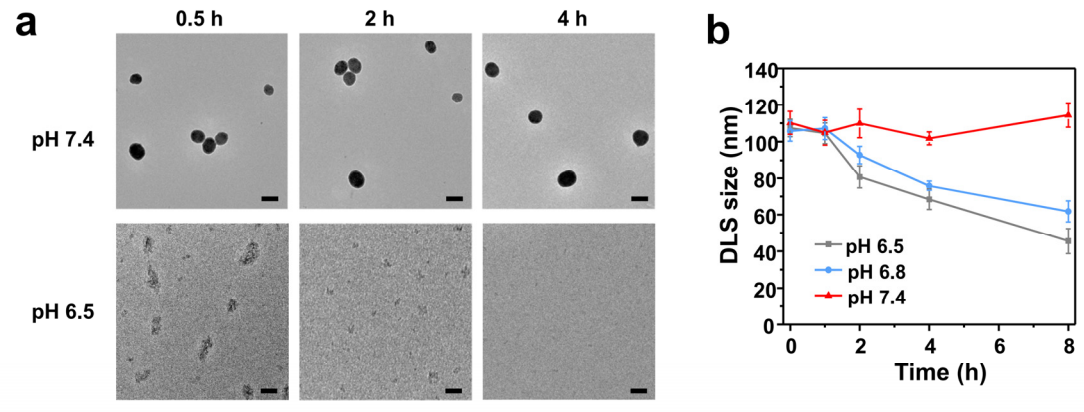

Supplementary Fig. 3. (a) Representative TEM images of aCD47@$CaCO_3$ NPs after being immersed in phosphate buffered saline (PBS) with different pH values (7.4 and 6.5) and for different periods of time (scale bar: 100 nm). The experiments were repeated three times. (b) Time-dependent DLS-measured size changes of aCD47@$CaCO_3$ NPs dispersed in PBS with different pH values (6.5, 6.8, and 7.4). Data are presented as mean ± s.e.m. (*n*=3).

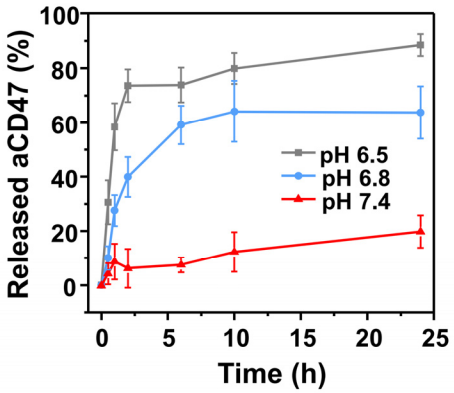

Supplementary Fig. 4. Time-dependent release profiles of aCD47 from $CaCO_3$ NPs dispersed in PBS with different pH values (6.5, 6.8, and 7.4). Data are presented as mean ± s.e.m. (*n*=3).

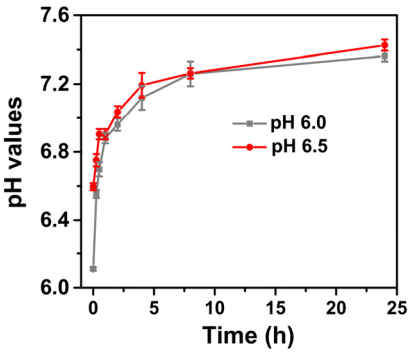

Supplementary Fig. 5. Time-dependent pH value changes of PBS containing $CaCO_3$ NPs. Data are presented as mean ± s.e.m. (*n*=3).

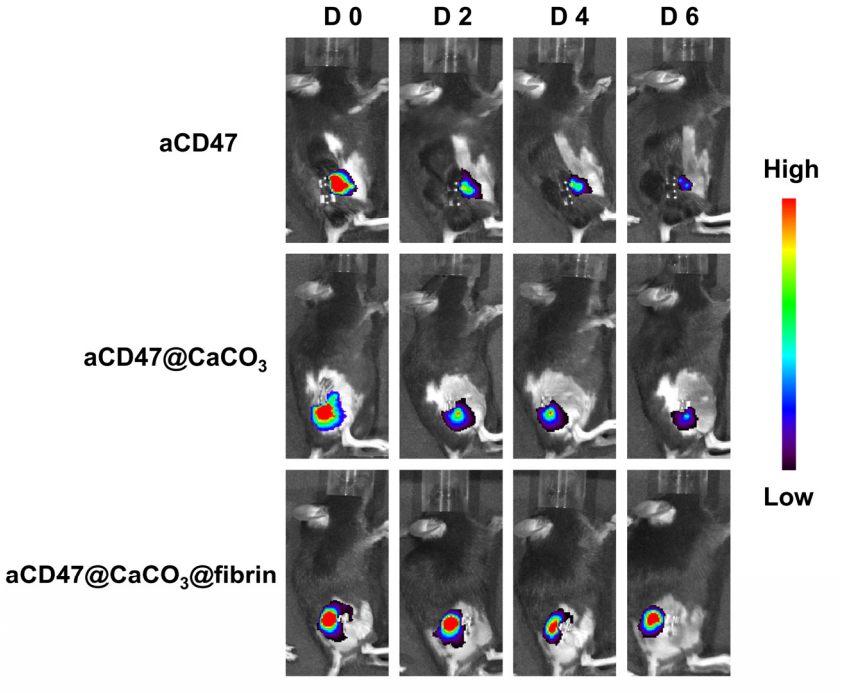

Supplementary Fig. 6. Fluorescence IVIS imaging depicting the *in vivo* retention profile of aCD47–Cy5.5 on different days post-antibody administration. The experiments were repeated three times.

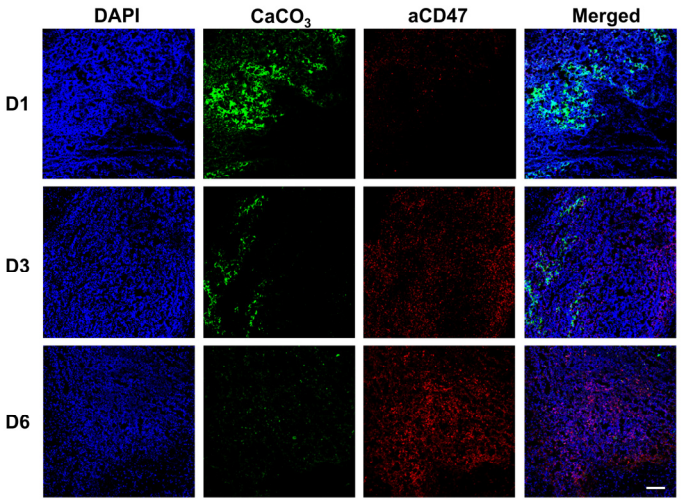

Supplementary Fig. 7. Confocal immunofluorescence images of tumours collected after treatment of aCD47@$CaCO_3$@fibrin at different time points (Scale bar, 50 μm). Green and red fluorescence indicate $CaCO_3$ NPs (FITC labelled PEG-b-P(Glu) copolymers) and aCD47 (rhodamine (TRITC))-conjugated anti-rat IgG antibody), respectively. The experiments were repeated three times.

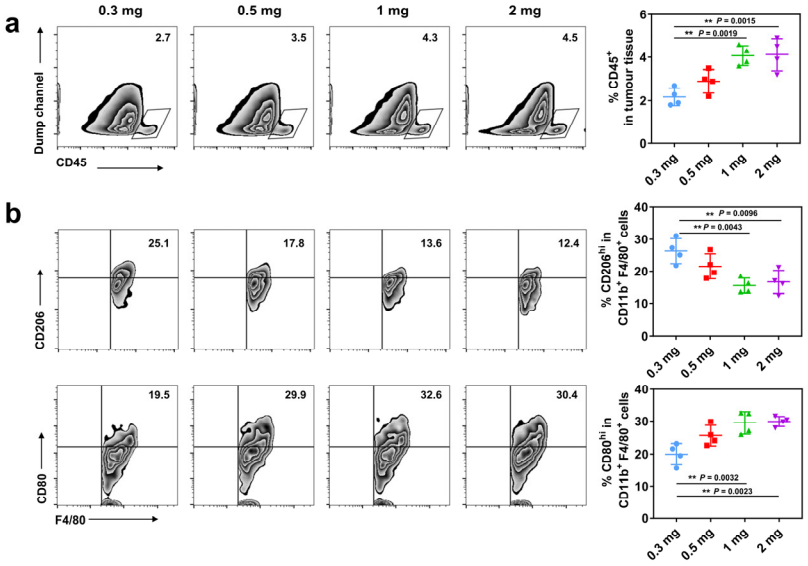

Supplementary Fig. 8. Dose effects of $CaCO_3$ nanoparticles on macrophage polarization. (a) Representative flow cytometry analysis (left) and the relative quantification (right) of $CD45^+$ cells after treatment with $CaCO_3$@fibrin at different amounts of $CaCO_3$ NPs. The data are presented as mean ± s.e.m. (n=4). (b) Representative flow cytometry analysis (left) and the relative quantification (right) of M2-like macrophages ($CD206^{hi}$) and M1-like macrophages ($CD80^{hi}$) gating on $F4/80^+CD11b^+CD45^+$ cells. Data are presented as mean ± s.e.m. (n=4). Statistical significance was calculated *via* one-way ANOVA with a Tukey post-hoc test. P value: $^*P < 0.05$; $^{**}P < 0.01$; $^{***}P < 0.001$.

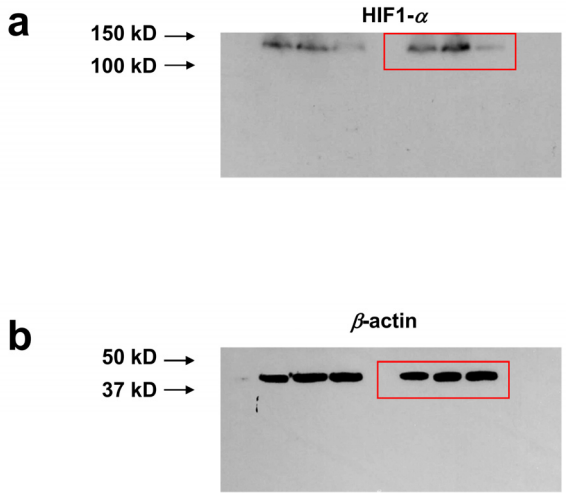

Supplementary Fig. 9. Uncropped western blots for Figure 2g. Lanes used for Figure 2g are indicated by red rectangles.

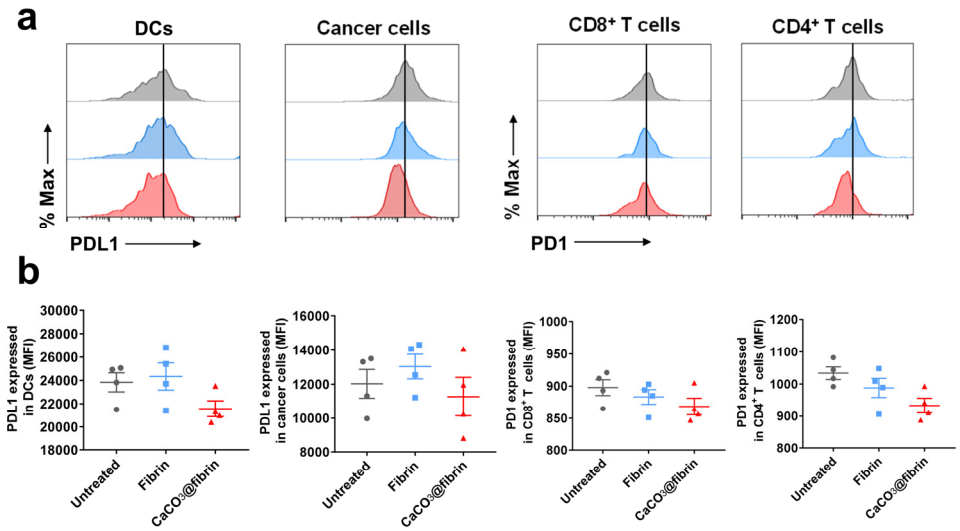

Supplementary Fig. 10. (a) PD-L1 expression of DCs gating on $CD45^+CD11c^+$ cells and tumour cells and PD-1 expression of tumour-infiltrating lymphocytes gating on $CD3^+$ cells after $CaCO_3$@fibrin treatment and (b) the corresponding quantification of PD-L1 and PD-1 mean intensity. Data are presented as mean ± s.e.m. *(n*=4).

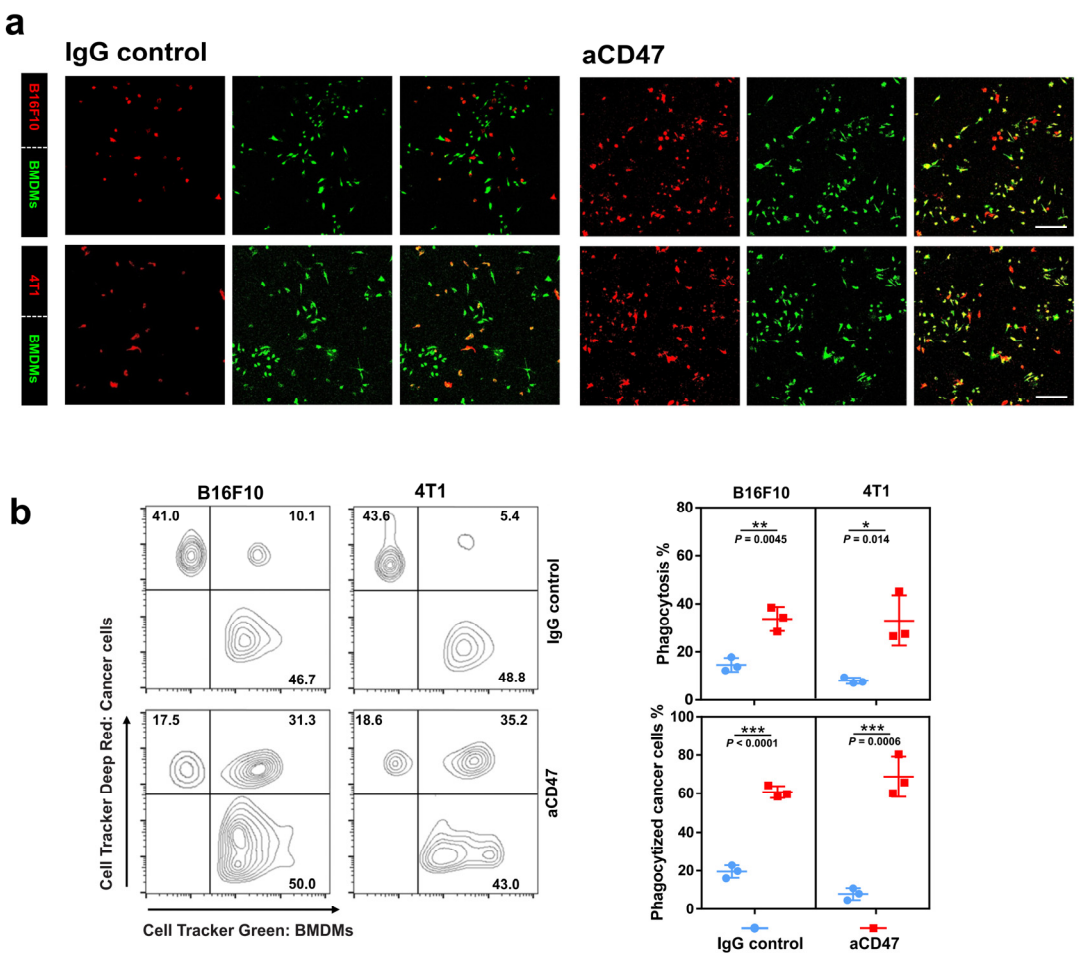

Supplementary Fig. 11. (a) Representative confocal images of phagocytosis assays in which cancer cells including B16F10 and 4T1 were labelled with CellTracker DeepRed and bone marrow derived macrophages (BMDMs) were labelled with CellTracker Green (Scale bar, 100 μm). The experiments were repeated three times. (b) Representative flow cytometric analysis images (left) and the corresponding quantification (right) of the phagocytosis of cancer cells (B16F10 and 4T1) by BMDMs. Phagocytosis or phagocytized cancer cells were quantified as the percentage of double-positive BMDMs among CellTracker Green-positive BMDMs or CellTracker DeepRed-cancer cells. Data are presented as mean ± s.e.m. (n=3). Statistical significance was calculated *via* two-tailed Student's t-test. P value: $^{*}P < 0.05$; $^{**}P < 0.01$; $^{***}P < 0.001$.

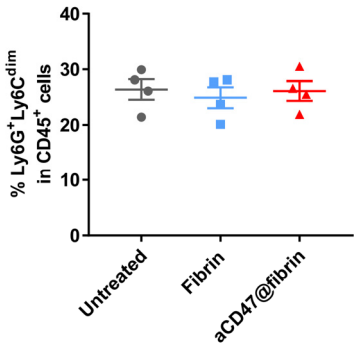

Supplementary Fig. 12. Percentage of $Ly6G^{+}Ly6C^{dim}$ neutrophils gating on $CD45^{+}$ cells. Data are presented as mean ± s.e.m. (n=4).

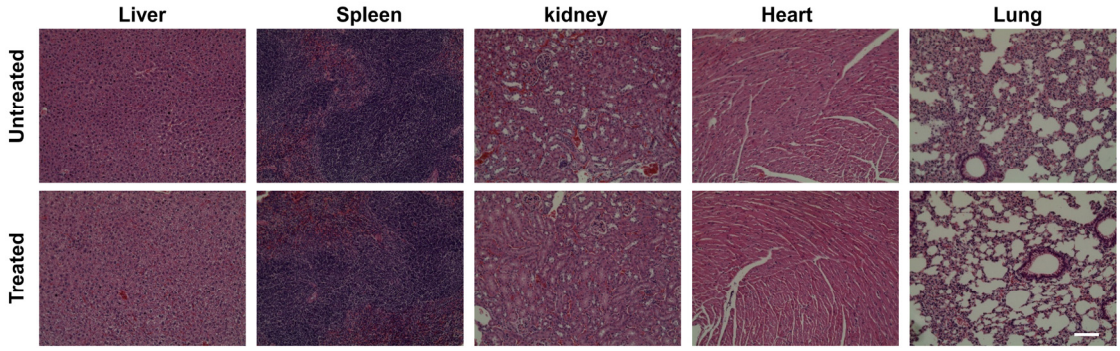

Supplementary Fig. 13. Haematoxylin and eosin (H&E) stained micrographs of major organs collected from healthy mice and aCD47@$CaCO_3$@fibrin treated mice at Day 30 (scale bar: 100 μm). The experiments were repeated three times.

	WBC (10^9/L)	RBC (10^{12}/L)	HGB（g/dL）	HCT（%）	MCV (fL)	MCH (pg)
Reference range	3.90~13.94	7.37~11.50	10.9~18.1	37.2~58.0	42.60~55.6	13.0~16.8
Healthy control	8.57±1.20	10.51±1.17	14.8±3.2	44.0±3.5	51.9±1.0	14.7±0.4
1D after treatment	7.15±2.11	8.28±1.89	11.8±0.9	46.4±6.4	51.1±3.8	15.3±0.5
7D after treatment	7.45±1.70	8.73±1.62	13.7±0.9	49.9±1.3	51.3±1.1	14.9±0.2
14D after treatment	6.95±0.98	9.68±0.50	14.0±1.7	49.0±4.2	50.6±1.9	14.8±0.3

	MCHC (g/dL)	PLT (10^9/L)	BUN (mmol/L)	ALT (U/L)	ALP (U/L)	AST (U/L)
Reference range	26.0~35.9	565~1849	5~26	27~195	105~370	43~397
Healthy control	27.9±0.7	659±59	19.9±3.3	163±14	132±10	95±50
1D after treatment	28.6±0.8	735±114	19.3±2.4	90±15	167±8.7	122±32
7D after treatment	29.0±0.7	775±79	21.9±2.6	134±50	151±22	120±37
14D after treatment	29.6±1.1	716±70	22.1±3.7	116±37	154±39	113±27

Supplementary Fig. 14. Female C57BL/6 mice were sacrificed at day 1, day 7, day 14 after aCD47@$CaCO_3$@fibrin treatment. Untreated healthy mice were used as a control. Complete blood counts: blood levels of white blood cells (WBC), red blood cells (RBC), hemoglobin (HGB), hematocrit (HCT), mean corpuscular volume (MCV), mean corpuscular hemoglobin (MCH), mean corpuscular hemoglobin concentration (MCHC). Serum biochemistry data including blood urea nitrogen (BUN) levels and liver function markers such as alanine aminotransferase (ALT), alkaline phosphatase (ALP), and aspartate aminotransferase (AST), were also measured. Data are presented as mean ± s.d. (n=4). Reference ranges of hematology data of healthy female C57BL/6 mice were obtained from Charles River Laboratories: (http://www.criver.com/).

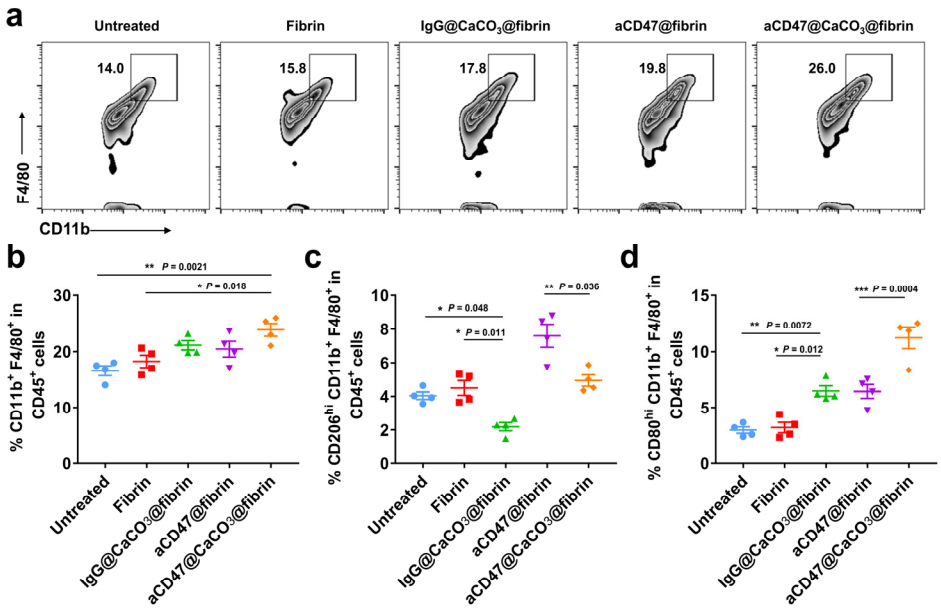

Supplementary Fig. 15. (a) Representative flow cytometric analysis images and (b) the corresponding quantification of F4/80^{+}CD11b^{+} macrophages gating on CD45^{+} cells. Data are presented as mean ± s.e.m. (n=4). (c) Percentage of M2-macrophages (CD206^{hi}) and (d) M1-macrophages (CD80^{hi}) in CD45^{+} cells. Data are presented as mean ± s.e.m. (n=4). Statistical significance was calculated *via* one-way ANOVA with a Tukey post-hoc test. P value: *$P < 0.05$; **$P < 0.01$; ***$P < 0.001$.

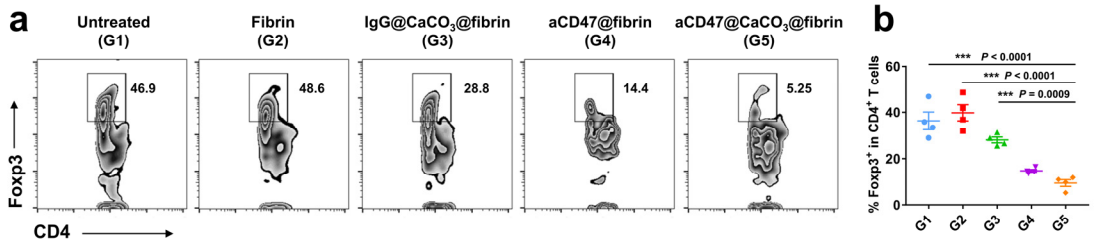

Supplementary Fig. 16. (a) Representative flow cytometric analysis images and (b) the corresponding quantification of CD4^{+}Foxp3^{+} T cells gating on CD3^{+}CD4^{+} cells after different treatments. Data are presented as mean ± s.e.m. (n=4). Statistical significance was calculated by one-way ANOVA using the Tukey post-test. P value: *, P<0.05; **, P<0.01; ***P<0.001.

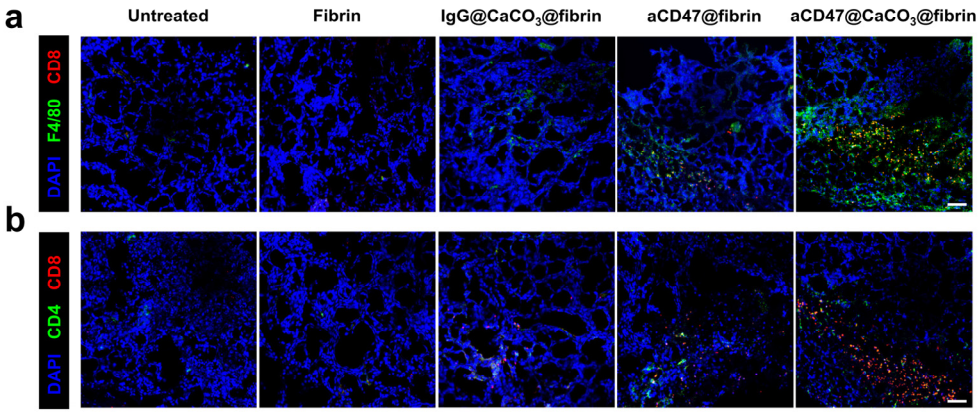

Supplementary Fig. 17. Representative immunofluorescence images of tumours showing $CD4^+$ T cell, $CD8^+$ T cell, and $F4/80^+$ macrophages infiltration for all five treatment groups (complete panel for Fig. 5e). Scale bar, 50 μm. The experiments were repeated three times.

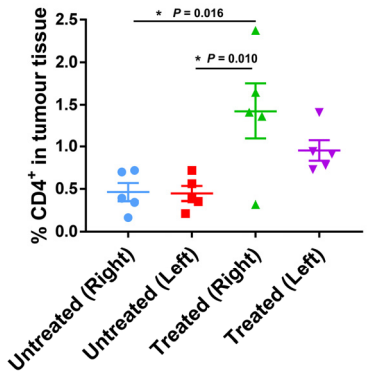

Supplementary Fig. 18. Absolute percentage of the $CD4^+$ cells in left and right tumours in untreated and treated mice. Data are presented as mean ± s.e.m. (n=5). Statistical significance was calculated by one-way ANOVA using the Tukey post-test. P value: *, P<0.05.

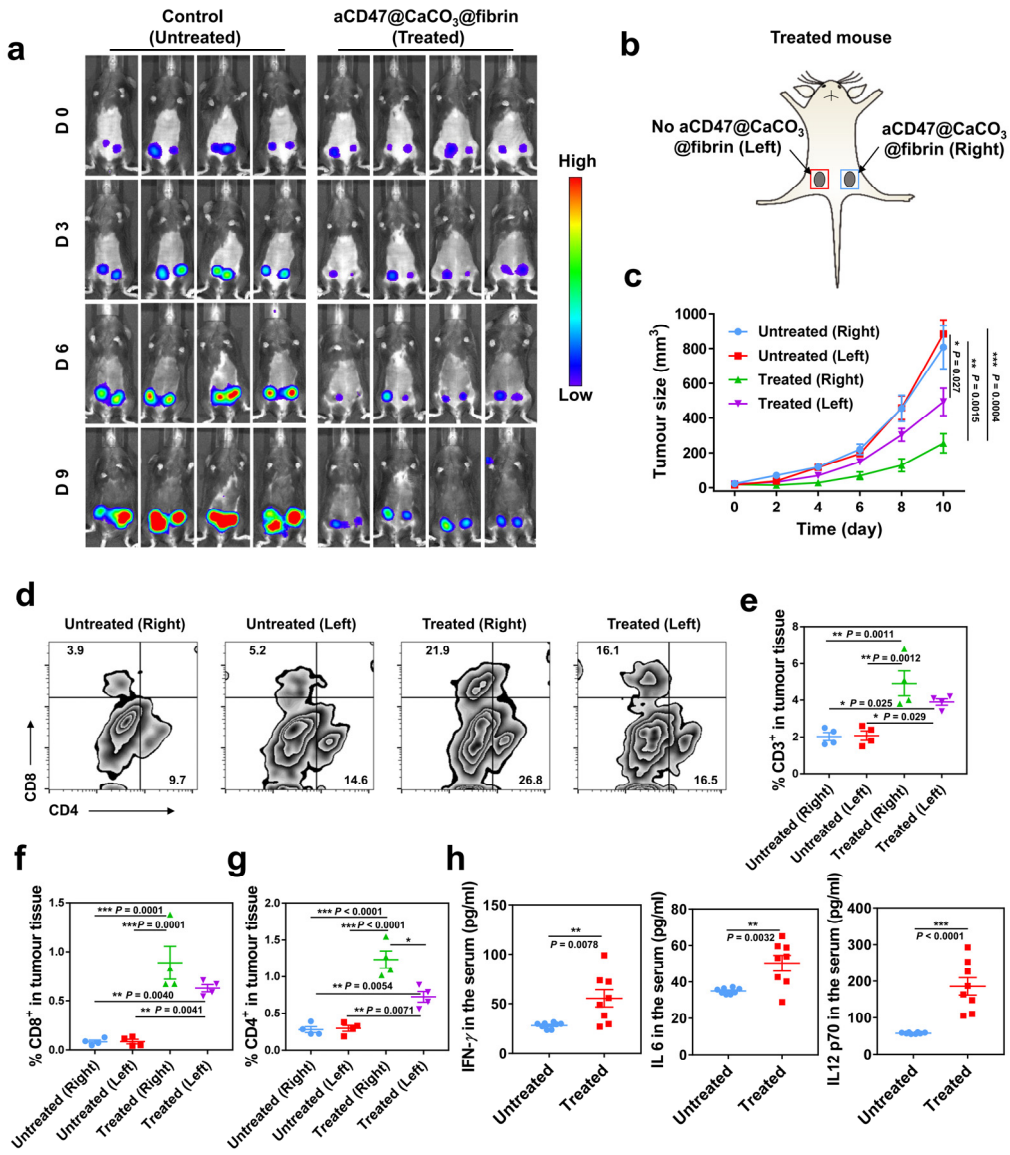

Supplementary Fig. 19. Peritumoural injection of aCD47@$CaCO_3$@fibrin for systemic anticancer immune response. (a) *In vivo* bioluminescence imaging of B16F10 tumours in response to local injection of aCD47@$CaCO_3$@fibrin hydrogels. The experiments were repeated three times. (b) Mice were inoculated with tumour cells both in the right and left flanks. Treated mice were implanted with hydrogels only on the right flank. (c) Left and right tumour growth curves in untreated and treated mice. Data are presented as mean ± s.e.m. (n=6). (d) Representative flow cytometric analysis of T cell infiltration within the tumour and (e) the relative quantification results in untreated and treated mice. Data are presented as mean ± s.e.m. (n=4). (f) Absolute percentage of $CD8^+$ and (g) $CD4^+$ T cells within tumours upon various treatments. Data are presented as mean ± s.e.m. (n=4). (h) Cytokine levels in the serum from mice collected five days after treatments. Data are presented as mean ± s.e.m. (n=8). Statistical significance was calculated *via* one-way ANOVA with a Tukey post-hoc test (c, e-g) or two-tailed Student's t-test (h). P value: $^*P < 0.05$; $^{**}P < 0.01$; $^{***}P < 0.001$.

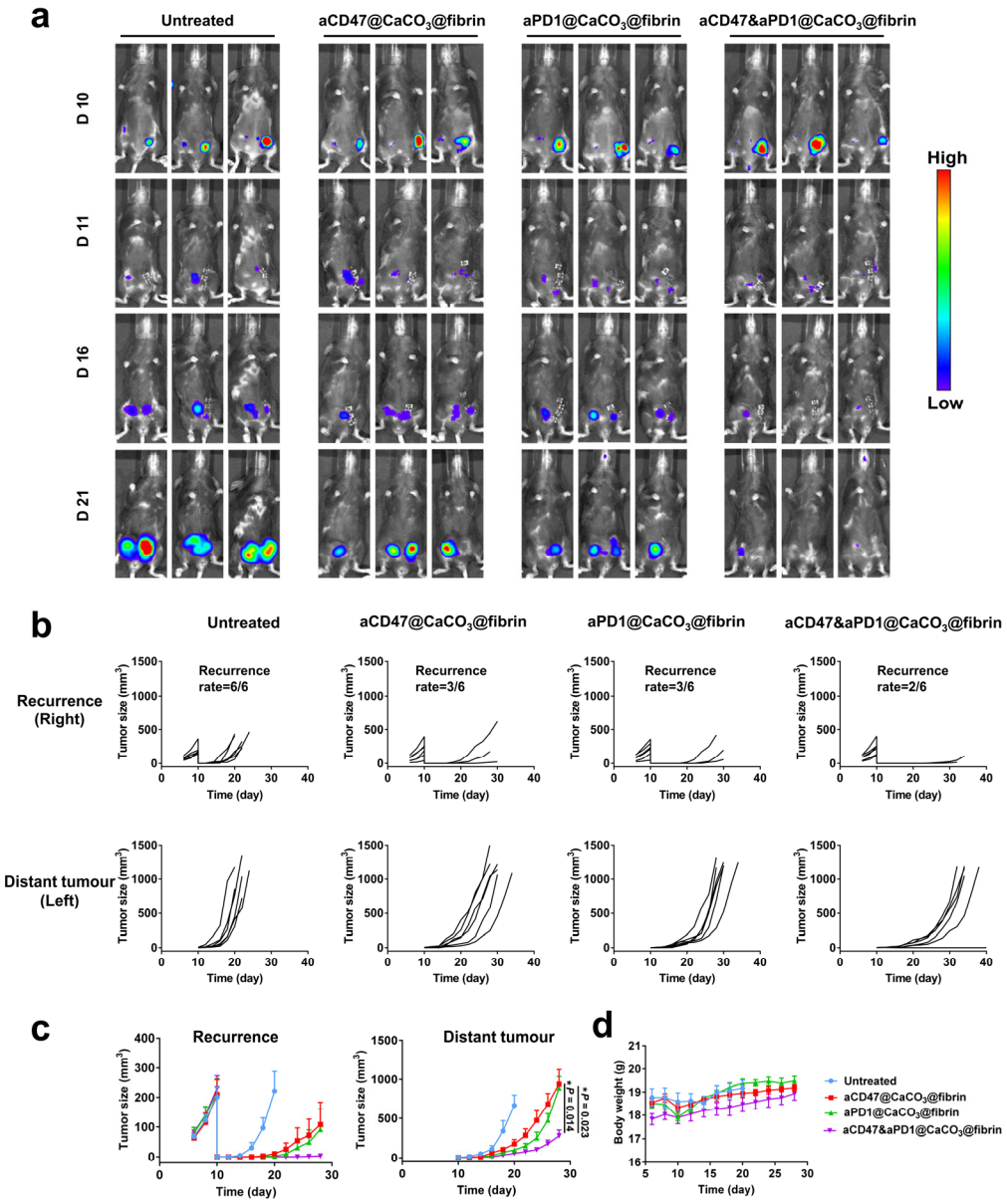

Supplementary Fig. 20. Inhibition of tumour recurrence and distant tumours with combination immunotherapy. (a) *In vivo* bioluminescence imaging of B16F10 tumours after different treatments. The experiments were repeated three times. (b) Individual and (c) average tumour growth kinetics in different groups. Data are presented as mean ± s.e.m. (n=6). Growth curves were interrupted when the first mouse of the corresponding group was euthanized. (d) Weight changes of the mice in different groups. Data are presented as mean ± s.e.m. (n=6). Statistical significance was calculated *via* one-way ANOVA with a Tukey post-hoc test. P value: $^{*}P < 0.05$.